JOURNAL OF Applied Polymer SCIENCE

Phase Behaviors of Diblock Copolymer/Nanorod Composites under Oscillatory Shear Flow

Linli He, Shiben Li, Linxi Zhang
Department of Physics, Wenzhou University, Wenzhou, People's Republic of China
Correspondence to: L. He (E-mail: helinli155@163.com)

ABSTRACT: The phase behaviors of lamellar diblock copolymers (DBCPs) melts and lamellar DBCPs/nanorods (NRs) composites subjected to oscillatory shear flow, have been investigated using dissipative particle dynamics. The oscillatory shear is a quite common shearing mode used in experiments and manufacturing processes. The rich lamellar (LAM) reorientation and morphological transition of systems strongly depend on the shear amplitude and shear frequency. At very low frequency, the amplitude-induced phase behaviors of DBCPs melts or DBCPs/NRs composites are quite similar to those subjected to a steady shear. For DBCPs/NRs case, we control NRs concentration low 15% to preserve LAM morphology in the nanocomposites, and simultaneously consider both types of selective and nonselective NRs. Our aim is to compare the different inductions on DBCPs melts or nanocomposites caused by shear amplitude and frequency, and observe how the NRs are oriented and dispersed in phase-separated copolymers matrix while under oscillatory shear, and how the presence of selective/nonselective NRs affects the shear-induced LAM reorientations and rheological properties of systems. Our results show the NRs orientation not only directly depend on the imposed shear flow but also is interfered by the alignment of shear-stretched copolymer molecules. The shear viscosity decreases with the frequency decreases, also influenced by the NRs concentration and surface property. © 2012 Wiley Periodicals, Inc. J. Appl. Polym. Sci. 000: 000–000, 2012

KEYWORDS: nanorod; oscillatory shear flow; dissipative particle dynamics simulation

Received 10 September 2011; accepted 9 May 2012; published online
DOI: 10.1002/app.38039

INTRODUCTION

Diblock copolymers (DBCPs) are polymers consisting of two mutually immiscible blocks (A and B) of polymers, chemically connected by the covalent bond. When a melt of these polymers is quenched, it forms rich-ordered microphase structures, lamellae and cylinders as well as spheres, and bicontinuous gyroid structures dependent on the block ratio, degree of incompatibility, temperature, etc.[1,2] However, in equilibrium such periodically ordered nanostructures can only be generated at mesoscopic scale, but disordered at macroscopic scale. The shear flow has been considered as an effective method for inducing long-range order,[3] structural transition,[4,5] and the orientation of self-assembled structures.[6,7] The lamellar (LAM) block copolymers systems subjected to steady[5–12] or oscillatory[13–17] shear flow are most-investigated. Koppi et al.[12] reported that near the order–disorder transition temperature (T_{ODT}), shear induced a new state into poly-(ethylenepropylene)–poly(ethylethylene) (PEP–PEE) lamellae, with their normals parallel to the vorticity axis (i.e., perpendicular alignment). Hadziioannou et al.[13] also showed that large-amplitude oscillatory shearing-oriented LAM microdomains parallel to the shearing surfaces, so that the normal to the lamellae was in the direction of the shearing gradient (i.e., parallel alignment). Conclusively, three typical LAM orientations have been summarized: the parallel (i.e., the LAM normal is parallel to the velocity gradient direction), the perpendicular (i.e., the LAM normal is perpendicular to the velocity gradient direction), and the transverse orientation (i.e., the LAM normal is parallel to the velocity direction). The reorientation between various LAM alignments has been proven to depend on the shear rate γ within steady shear (or the shear amplitude γ_0 and frequency ν within oscillatory shear).[7,13] For steady-shear flow, it was observed experimentally that the LAM structures adopted parallel alignment at low-shear rates and perpendicular alignment at high-shear rates, and that it was possible to use shear with varied rates to induce a transition between the parallel and perpendicular alignment.[11] Besides the efforts in experiments, a lot of computational,[5–9] and theoretical[10] works have been carried out for elucidating the relation between the polymer phase behavior and shear rate for steady-shear case. However, in experiments and manufacturing processes, the more common shearing mode is the oscillatory shear. The complex orientation selection depending of shear amplitude and frequency has also been explored in some experiments,[13–17]

theories,[18,19] and simulations.[20,21] Wiesner et al.[14–16] investigated the lamellar PS-b-PI diblock copolymers and first constructed an orientation diagram as a function of shear amplitude and frequency. At low amplitude, parallel orientation was observed irrespective of frequency. At large amplitude, they identified two frequency regimes: in the high-frequency regimes shearing led to parallel orientation, whereas at low frequencies, it resulted in perpendicular orientation of the lamellae. Fraaije et al. theoretically described the reorientation phenomena in the LAM block copolymer melts under oscillatory shear. Their observations showed that the oscillating flow anisotropically suppressed fluctuations and gave rise to the parallel-to-perpendicular transition.[19]

Recently, the organic block copolymer and inorganic nanoparticle composites have attracted considerable attention as advanced engineering materials.[22,23] Especially, the anisotropic particles, such as nanorods (NRs), can display special characteristics in optical and electric properties, depending on the 1D orientational entropy. Experimentally, Huynh and Greene et al. found the solar cells that consisted of organic polymers and inorganic NRs displayed better efficiencies than general organic photovoltaic cells, resulted from that the long axis of NRs played as a continuous channel for transferring electrons, advantage over the nanospheres where electron hopping happened between particles.[24,25] Therefore, the research works on the distribution and orientation behaviors of NRs in polymer matrix, is very meaningful. Recent investigators have utilized the self-assembly characteristics of block copolymers to manipulate the phase behaviors of NRs within polymer fliuds.[26–28] Theoretically, Ma et al. constructed the phase diagrams of diblock/rod hybrids with different aspect ratio of particles, and regulated the particles' position and orientation distributions by varying the concentration of particles.[27] In our recent simulation studies on DBCP/nanorod mixtures under equilibrium conditions, the results that rich self-assembly structures of nanocomposites and phase behaviors of NRs (containing the orientation and distribution), could be further interpreted by the competition between enthalpy and entropy. The former involves the interactions between blocks and NRs, while the latter contains the orientational entropy of NRs, the configurational entropy of the chains, and the spatial confinement of phase-separated domains.[28]

As mentioned above, block copolymer/nanorod mixtures under equilibrium conditions have received considerable attentions, but investigations focusing on the phase behaviors of block copolymer/nanorod mixtures in out-of-equilibrium conditions, e.g., imposed by shear flow, are comparatively few. Undoubtedly, the internal mechanism of block copolymer/nanorod composites subjected to shear is more complex than that in equilibrium. It can be ascribed to the cooperative interplays between the shear-induced phase behaviors from polymer chains and NRs, respectively. A detailed study on this aspect will provide a good understanding of how NRs behave when shear is used to generate long-range order in block copolymer templates. Based on the published reports survey, only a handful of publications have directly addressed the block copolymer/nanoparticle systems in nonequilibrium, only limited to the case of spherical nanoparticles.[29–33] For example, Kalra et al.[29] simulated the lamellar DBCPs/nanoparticles mixtures imposed by steady shear. They summarized that the imposed shear flow could be as a beneficial mean to arrange nanoparticles into 3D ordered arrays within diblock templates, and meanwhile the loading of particles significantly influenced the shear-induced reorientation of LAM structure. Mendoza et al.[30,31] also used shear flow to organize gold nanoparticles into 3D ordered arrays within spherical, cylindrical, and lamellar structure of PS-b-P4VP diblock templates. Similar works were reported independently by Pozzo and Walker,[32,33] for micelle-crystal phases (spherical or cylindrical) incorporated by nanoparticles, in which the shear flow induced the particles into ordered arrays with a certain orientation. In photoelectric materials, the high aspect-ratio NRs favorably display the anisotropic behavior, which have been extensively applied in novel organic–inorganic solar cells, such as polymer/rod cells. However, investigations on the DBCPs/anisotropic NRs composites subjected to shear flow are relatively rare.

In our recent studies,[34,35] we have already tried to explore the effects of steady shear on the lamellar or cylindrical DBCPs and NRs composites. In the former case, we investigated the shear rate-induced self-assembly of composites loaded with low and high NRs concentrations. It is concluded that the self-assembled behaviors of composites, including NRs in polymer matrix, not only depend on the imposed shear rate but also significantly affected by the properties of NRs. The competitions between shear rate-induced phase behaviors from NRs and polymers are co-responsible for the rich reorientations and morphology transitions of systems.[34] In the latter studies, we focused on the mixtures of cylindrical DBCPs and NRs under both equilibrium and nonquilibrium conditions (i.e., implied by shear flow). First, NRs induced a series of self-assembly structures, including cylindrical, ribbon, and lamellar phases. Then, the steady shear with different flow directions and strengths was imposed initially to those equilibrium structures. Subjected to z-axis shear, the morphologies of nanocomposites were persisted, where NRs could be arranged in hexagonal packing arrays; Subjected to *x*-axis shear, the phase behaviors of DBCPs/NRs composites mainly depended on the NRs concentration.[35] However, the steady shear is the only simple process occurring in a typical polymer processing context, not as common as the oscillatory shear used in the experiments and manufacturing processes of the polymer materials. In this study, we use dissipative particle dynamics (DPD) simulations to investigate the lamellar DBCPs and NRs mixtures subjected to the oscillatory shear. Compared to our previous studies on the simple steady-shear case,[34,35] in this study, we comprehensively consider the sheared inductions on nanocomposites from amplitude and frequency, and analyze the inherent mechanisms of amplitude-induced and frequency-induced phase behaviors, respectively. In addition, similar to experiment studies, to investigate the different effects from interactions between components in the system, one can chemically coat the surface of the added particles with short polymeric ligands. For example, one could synthesize "A-selective" NRs by chemically modifying the rod surfaces with ligands of block A; in another scenario, one could chemically tether ligands of both blocks A and B on rod surfaces to fabricate

"nonselective" NRs. In our simulation, we model the selective/nonselective NRs by varying the attraction between A (or B) blocks and NRs. We focus on three issues: (1) how does LAM reorientations and morphological transitions of composites depend on shear amplitude and frequency? (2) How does oscillatory shear affect the phase behaviors of NRs (i.e., the positional distribution and spatial orientation)? (3) How does the loading of NRs (with varied concentrations and surface properties) affect the LAM reorientations and rheological properties of systems?

MODEL AND SIMULATION METHODS

The DPD method proposed by Hoogerbrugge[36] is appropriate for the investigation of the generic properties of macromolecular systems, such as polymer melts and solutions. It is also applicable to study the disorder–order and order–order transitions of polymer melts under shear conditions.[7,9,20] In DPD simulation, the "beads" or particles represent a cluster of atoms or molecules, which interact with each other via conservative force ($\vec{F}_{ij}^{C}$), dissipative force $\left(\vec{F}_{ij}^{D}\right)$, and random force $\vec{F}_{ij}^{R}$.

$$\vec{f}_i = \sum_{i \neq j} \left(\vec{F}_{ij}^{C} + \vec{F}_{ij}^{D} + \vec{F}_{ij}^{R} \right) \tag{1}$$

$$\vec{F}_{ij}^{C} = a_{ij}\omega(r_{ij})\hat{r}_{ij} \tag{2}$$

$$\vec{F}_{ij}^{D} = -\gamma\omega^2(r_{ij})\left(\hat{r}_{ij}\cdot\vec{v}_{ij}\right)\hat{r}_{ij} \tag{3}$$

$$\vec{F}_{ij}^{R} = \sigma\omega(r_{ij})\theta_{ij}\hat{r}_{ij} \tag{4}$$

where $\vec{r}_{ij} = \vec{r}_i - \vec{r}_j$, $r_{ij} = |\vec{r}_{ij}|$, $\hat{r}_{ij} = \vec{r}_{ij}/r_{ij}$, and $\vec{v}_{ij} = \vec{v}_i - \vec{v}_j$. $\omega(r)$ is a weight function, for which we adopt the commonly used form: $\omega(r_{ij}) = 1 - r_{ij}$ for $r_{ij} < 1$ and $\omega(r_{ij}) = 0$ for $r_{ij} \geq 1$. The conservative force $\vec{F}_{ij}^{C}$ is the soft repulsion potential within a certain cutoff radius r_c, where a_{ij} is a maximum repulsion between beads i and j. The combination of the dissipative and random forces ($\vec{F}_{ij}^{D}$ and $\vec{F}_{ij}^{R}$) constitutes a thermostat, where θ_{ij} is a randomly fluctuating variable with Gaussian statistics: $\langle\theta_{ij}(t)\rangle = 0$ and $\langle\theta_{ij}(t)\theta_{kl}(t')\rangle = (\delta_{ik}\delta_{jl} + \delta_{il}\delta_{jk})\delta(t-t')$. The fluctuation–dissipation theorem requires that σ and the friction parameter γ are related through the relation:

$$\sigma^2 = 2\gamma k_B T \tag{5}$$

where k_B is the Boltzmann's constant and T is the temperature. For convenience, the cutoff radius r_c, the energy k_BT and the particle mass m are all taken as unity. Referring to the classical DPD studies by Groot,[37] in this study, we set $\gamma = 6.57$, so $\sigma = 3.63$ according to eq. (5). In addition, for the polymers, the extra spring force $\vec{f}_i^{S}$, which acts between the connected beads in a chain, has the form of

$$\vec{f}_i^{s} = \sum_j C\vec{r}_{ij} \tag{6}$$

where C is a harmonic type spring constant, chosen to be equal to 4.0 in this study (in terms of k_BT).

For the rigid NRs, according to the previous studies,[28,38] it can be successfully constructed by a number of DPD beads (N_b) arranged in a straight line, with a fixed small distance (D_{b-b}) between consecutive beads, so that the length of NRs can be equivalently expressed as $L_r = (N_b - 1) \times D_{b-b}$. To avoid the undesired overlap between fluid particles and NRs, the number density of the DPD particles in a rod is larger than that of the fluids. We select $D_{b-b} = 0.3$ with a fixed $N_b = 6$, so the NRs length L_r is fixed to 1.5 according to the definition. Moreover, the ratio of L_r/L_0 (NRs length/period width of DBCPs melts) is about 0.33,[28] compared with the experimental ratio range of $L_r/L_0 = 10\text{–}60$ nm/60 nm = 0.17–1.0.[26] Moreover, for NRs dynamics process, a constraining routine is used to keep the inner particles aligned and equidistant during the simulation. In brief, the forces on the DPD particles of a rod are converted into a net force on the two end DPD particles, and the equations of motion for these two DPD particles are solved, using the standard shake routine to keep them at a fixed distance. The positions of the N_b-2 intermediate DPD particles are then readily calculated by a linear interpolation at the end of each timestep.[38] The Newton equations for all particles' positions and velocities are integrated by a modified version of the velocity Verlet algorithm.[39]

Our simulation system consists of the symmetric DBCPs melts (A_5B_5) and NRs (selective and nonselective). The number density of the fluid system is $\rho = 5$, and then the repulsive parameter a_{ij} in eq. (2) relates to the Flory–Huggins χ-parameter, via

$$a_{ii}\rho = 75k_BT \tag{7}$$

$$a_{ij} \approx a_{ii} + 1.45\chi_{ij}(\rho = 5) \tag{8}$$

where the repulsion parameter between particles of the same type $a_{ii} = 15k_BT$ to correctly describe the compressibility of the water.[39] In this study, the values of a_{ij} between the three types of DPD beads (represented by A, B, and R), are given by $a_{AA} = a_{BB} = 15$ and $a_{AB} = a_{RR} = 30$. Meanwhile, the values of a_{AR} and a_{BR} depend on the selectivity of NRs to blocks. The A-selective NRs corresponds to $a_{AR} = 15$ and $a_{BR} = 30$ (i.e., preferential to A blocks), while nonselective NRs corresponds to $a_{AR} = 15$ and $a_{BR} = 15$(i.e., no preferential to both blocks), where the corresponding NRs concentrations for selective and nonselective are defined by ϕ_A and ϕ_N, respectively.

To impose the external oscillatory shear flow, we use the SLLOD (so named because of its close relationship to the Dolls tensor) algorithm so that the motion equations of particles are modified as follows:[40]

$$\dot{\vec{r}} = \vec{p}_i/m + \hat{i}\dot{\gamma}\, r_{yi} \tag{9}$$

$$\dot{\vec{p}}_i = \vec{F}_i - \hat{i}\dot{\gamma}\, p_{yi} \tag{10}$$

where $\vec{r}_i$ and $\vec{p}_i$ is the position and the momentum of particle i, respectively. $\hat{i}$ is the unit vector in the x-axis direction and $\dot{\gamma} = \partial v_x/\partial r_y$ is the shear rate. The flow direction is parallel to the x-axis, the y-axis refers to the velocity gradient, and the z-axis represents the transverse direction. Meanwhile, we use the

Lees–Edwards periodic boundary condition to control and maintain the oscillatory shear flow,[41] wherein two opposing periodic images are incrementally moved in opposite directions consistent with the imposed shear. The modified equations of motion are integrated with the time step of $\Delta t = 0.04\tau_0$, where τ_0 is the natural DPD time unit defined as $r_c\sqrt{m/k_BT}$.[39] We introduce the sinusoidally changing shear rate in the form of $\dot{\gamma}(t) = \gamma_0 \cos(\omega t)$, where γ_0 is the oscillatory shear amplitude and $\omega = 2\pi v$, with v being the oscillatory shear frequency.[41] Well compared with previous studies on the steady-shear flow,[34] in this study, the maximum value of shear amplitude is also set as $\gamma_0 = 0.21$, to avoid the potential microturbulence and distortion. In our simulations, while the cycle of the oscillatory shear takes the value ranged from 2.0×10^2 to $2.0 \times 10^5 \Delta t$ (i.e., from 8.0 to $8.0 \times 10^3 \tau_0$), corresponding frequency v is ranged from 5.0×10^{-3} to $5.0 \times 10^{-6} \Delta t^{-1}$,[41] which are divided into three frequency regimes: high, intermediate and low frequency regions. Based on the published reports,[42] the relaxation time τ of the chain is calculated to be $11.9\tau_0$ by fitting the end-to-end vector autocorrelation function. Correspondingly, in this study, a cycle of the oscillatory shear are roughly calculated as ranged from τ to 670τ, so our chosen shear frequencies are controlled within a reasonable range in the simulations.

The simulations are performed in a cubic box of constant volume $V = 11 \times 11 \times 11$, with periodic boundary conditions applied in all three directions. The simulated systems contain $N_p \equiv \rho V = 6655$ polymer DPD beads and $N_p \phi_R/(1 - \phi_R)$ rod DPD beads for the number density $\rho = 5$, where ϕ_R represents the concentration of NRs. Before subjected to oscillatory shear flow, first, A_5B_5 melts and NRs are randomly dispersed in the simulated box, the stable LAM phases of A_5B_5/NRs composites are obtained at least over 1.0×10^6 timestep and independent of the initial state. Then, the stable LAM phase of composites are replaced transverse to the shear direction (i.e., the lamellar normal is parallel to the velocity direction), which are defined as the starting state. After imposed by the oscillatory shear flow, 2.0×10^6 timestep are performed in the nonequilibrium simulations, which includes at least 10 oscillatory shear cycle. To eradicate the finite-size effect, some extra simulations have been carried out by enlarging the box size to $V = 13 \times 13 \times 13$ ($N_p = 10985$), also starting from the same quiescent state. After much longer simulation time, similar results are found, which will be discussed in detail in the following section. In addition, the complex shear viscosity η is calculated based on the xy-component pressure tensorP_{xy}, of which the real part is given by:[43]

$$\eta(v) = -\frac{1}{\gamma_0 t}\int_0^t ds \cos(vs) P_{xy}(s) ds \tag{11}$$

RESULTS AND DISCUSSION

Recently, we studied the lamellar DBCPs/NRs composites under equilibrium conditions (i.e., without shear).[28] For the case of selective NRs, with varying the NRs concentration, we observed the rich morphological transitions from lamellar to lamellar/cylindrical mixed to cylindrical, even to elliptic structures, and etc; for case of nonselective NRs, no order–order morphology transitions was induced but order–disorder transition, because of the reduction in segregation $(\chi N)_{eff}$between A and B blocks caused by the NRs' preferential distribution in AB interface. To readily compare both the cases of DBCPs/NRs systems under equilibrium and nonequilibrium conditions, in this study, all stable states before shearing whether DBCPs melts or nanocomposites, are corresponding to the morphology phase diagram in the published reports.[28] In short, with the loading of NRs into DBCPs melts, the instinct aggregates and orientation behaviors of NRs confined to DBCPs phase-separated regions would lead to an isotropic-nematic (IN) transition, and then induce a series of phase transitions. To preserve LAM structure in the nanocomposites, we control the NRs concentration below 15%, divided into three cases: (1) pure DBCPs melts with $\phi_{A(N)} = 0\%$; (2) low NRs concentration with $\phi_{A(N)} = 5\%$; (3) high NRs concentration with $\phi_{A(N)} = 15\%$.

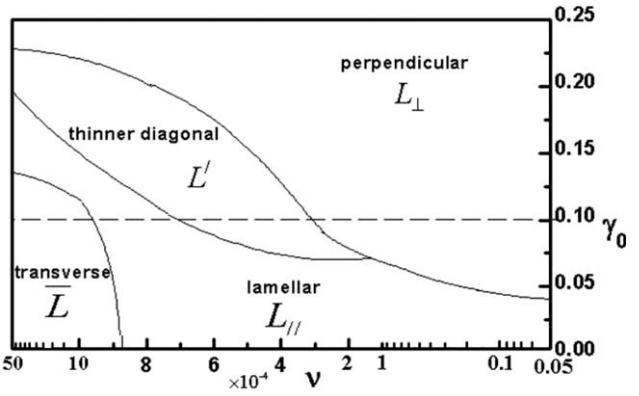

Figure 1. Orientational diagram of lamellar DBCPs melts under oscillatory shear at different amplitudes γ_0 and frequencies v.

Pure DBCPs Melts

We first investigate the effects of oscillatory shear on the self-assembly of A_5B_5 melts. With simulations on the continuous variation of shear amplitude and shear frequency, we roughly construct a LAM orientation diagram in Figure 1, indicating the dependence of LAM orientation on the amplitude and frequency. Concretely, the corresponding density profiles of diblocks are used to distinguish the LAM phase belonged to different alignments. Horizontally, the whole frequency range is divided into three regimes: high, intermediate, and low frequency. Although the frequency range from 1.0×10^{-3} to 1.0×10^{-4} is enough to show the effects of shear frequency on LAM reorientation, here the frequency range is extended widely from 5.0×10^{-3} to 5.0×10^{-6}, so as to consider the two extreme cases: the higher (high to 5.0×10^{-3}) or the lower (low to 5.0×10^{-6}) shear frequency. For simplicity, we use the log-scale for shear frequency v in the phase diagram of Figure 1, equivalently ranged from 50×10^{-4} to 0.05×10^{-4}, to comprehensively investigate the shear frequency in high, intermediate, and low regimes. Under the two extreme cases, the system imposed by shearing would present the special physical meaning, which is self consistent with the previous studies.[10,20] If the shear frequency is too high, for instance, $v = 1.0 \times 10^{-3}$, it is too fast to have enough time to relax the polymer chain, therefore no

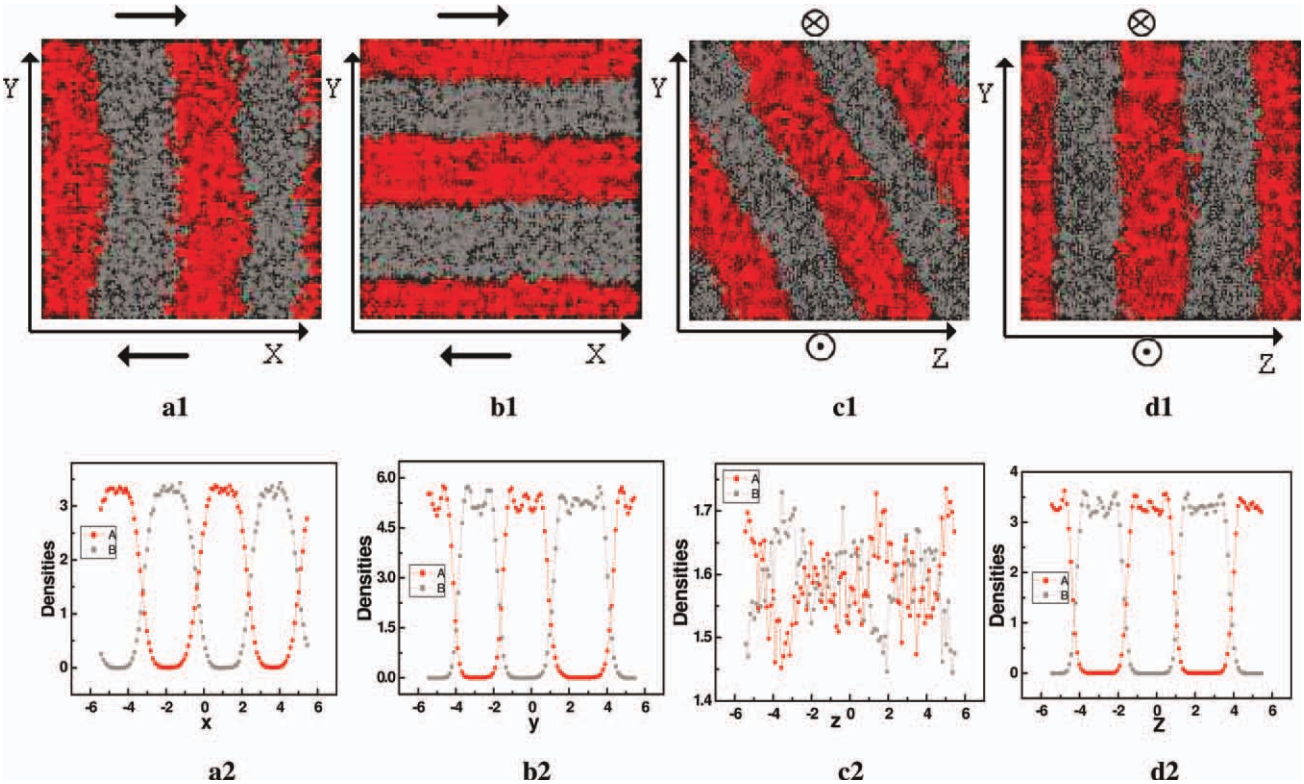

Figure 2. Morphologies and densities of lamellar DBCPs melts at amplitude $\gamma_0 = 0.1$ and frequencies $v = 1.0 \times 10^{-3}$, 8.0×10^{-4}, 5.0×10^{-4}, and 2.5×10^{-4}. A and B blocks are presented in gray and red, respectively. The arrows show the imposed shear direction, parallel to *x*-axis. The view in (a1–b1) is perpendicular to shear direction, while the view in (c1–d1) is parallel to shear direction. [Color figure can be viewed in the online issue, which is available at wileyonlinelibrary.com.]

LAM reorientation or phase transition is observed during shear, and the initial transverse LAM ($\bar{L}$) is always preserved. To the other extreme, if the shear frequency is too low, for example, $v = 1.0 \times 10^{-5}$ or even 5.0×10^{-6}, the reorientations of LAM phase completely depend on the shear amplitudes, i.e., LAM phase preferentially adopts parallel alignment at low-shear amplitudes and perpendicular alignment at high-shear amplitudes, which is similar to the case of those subjected to the steady shear,[10] dependent on the shear rate. Longitudinally, the perpendicular orientation is always preferred at large-shear amplitudes; at low-shear amplitudes, parallel orientation is observed irrespective of frequency; at intermediate shear amplitudes, for example, $\gamma_0 = 0.1$, the shear frequency plays an important role in the orientation selection of LAM phase. As shown in Figure 2(a1–d1), we present the typical snapshots of lamellar DBCPs melts with different frequencies $v = 1.0 \times 10^{-3}$, 8.0×10^{-4}, 5.0×10^{-4}, and 2.5×10^{-4}, corresponding to transverse LAM ($\bar{L}$), parallel LAM ($L_{//}$), thinner diagonal LAM ($L^{/}$), and perpendicular LAM ($L_{\perp}$) structures, respectively. The strongly segregated blocks within ordered lamellae are clearly visualized by the A/B density profiles in Figure 2(a2–d2). At very high frequency ($v = 1.0 \times 10^{-3}$, a1), one oscillatory cycle is less than the relaxation time of the polymer chain, so no LAM reorientation takes place except keeping the initial transverse alignment. The LAM orientation transition from transverse alignment to parallel alignment is observed at high frequency ($v = 8.0 \times 10^{-4}$, b1), and comparatively, the reorientation from transverse LAM to perpendicular LAM appears at low frequency ($v = 2.5 \times 10^{-4}$, d1), in good agreement with the experimental studies by Wiesner et al.,[16] as well as the theory calculations of Chen et al.[18] The oscillatory shear-induced LAM reorientation is quite different from that in steady-shear case, where the LAM orientation is perpendicular at strong shear rate and parallel at weak shear rate.[7] In addition, there is a transient LAM phase between parallel and perpendicular orientation, i.e., diagonal LAM structure (with the lamellae oriented in the shear direction but diagonally between a parallel and perpendicular alignment, $v = 5.0 \times 10^{-4}$, c1), also observed frequently in the case of steady shear[7,8] Interestingly, from Figure 2(c1), we can clearly see the thinner layers, reflected by the fact that the number of the layers in the simulation box is increased under oscillatory shear. This shear thinning of polymer chains is attributed to the shear-induced suppression of concentration fluctuations,[16] which is a common characteristics existing in shear flow.

Low NRs Concentration

In this study, we study the effects of oscillatory shear on the phase behaviors of lamellar DBCPs and A-selective NRs mixtures, with the NRs concentration of $\phi_A = 5\%$. Also take shear amplitude $\gamma_0 = 0.1$, for examples, since at this amplitude, the LAM orientations are totally distinct at the three frequency

Applied Polymer SCIENCE

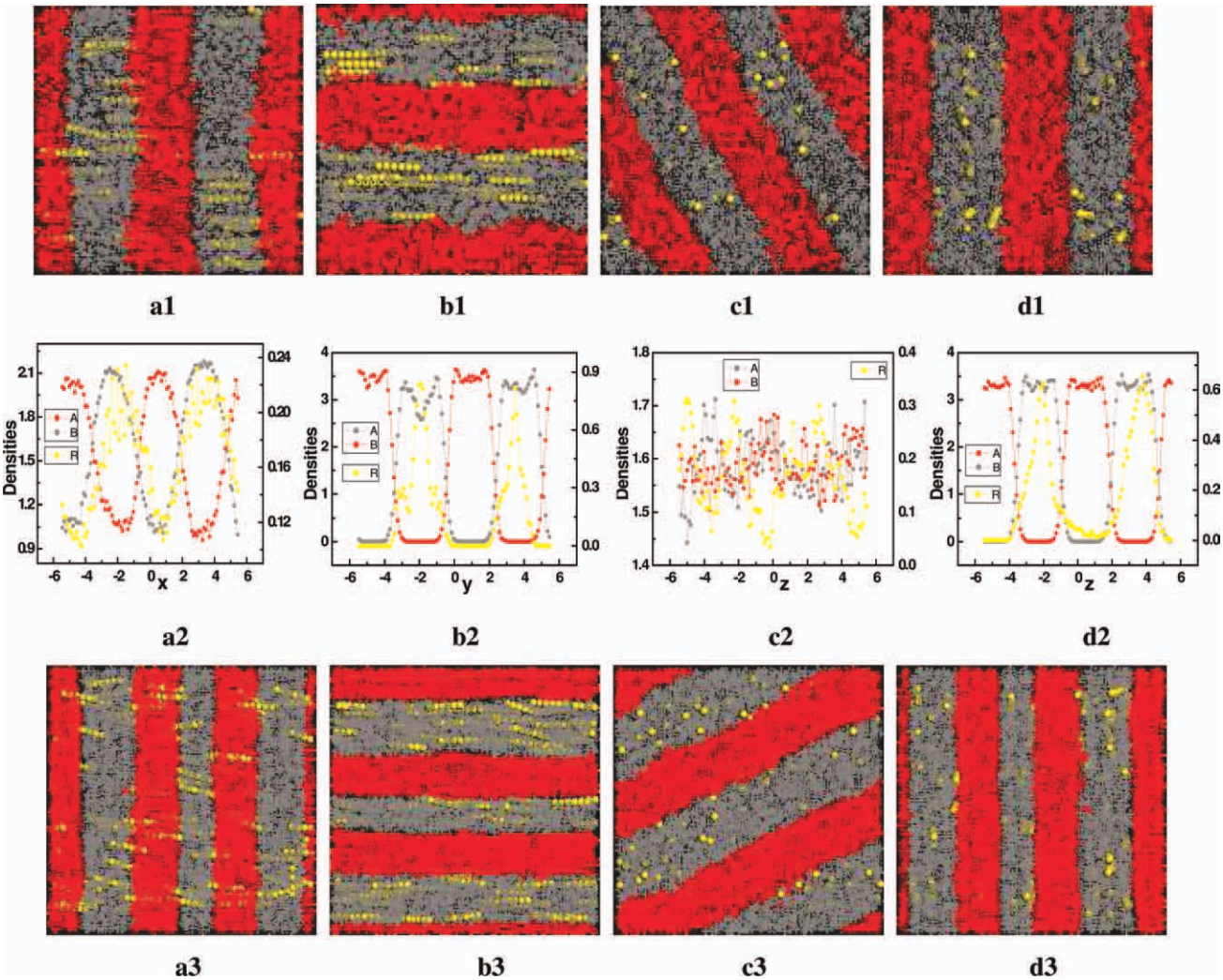

Figure 3. Morphologies and densities of DBCPs/A-selective NRs ($\phi_A = 5\%$) at amplitude $\gamma_0 = 0.1$ and frequencies $v = 1.0 \times 10^{-3}$, 8.0×10^{-4}, 5.0×10^{-4}, 1.5×10^{-4}. The corresponding simulations for $13 \times 13 \times 13$ DPD units systems are also shown in (a3–d3). In this study, NRs are presented in yellow. The view in (a1–b1) is perpendicular to shear direction, while the view in (c1–d1) is parallel to shear direction. [Color figure can be viewed in the online issue, which is available at wileyonlinelibrary.com.]

regimes considered in this study. In Figure 3(a1–d1), we show simulation snapshots of nanocomposites at different frequencies of $v = 1.0 \times 10^{-3}$, 8.0×10^{-4}, 5.0×10^{-4}, and 1.5×10^{-4}, corresponding to transverse LAM, parallel LAM, thinner diagonal LAM, and perpendicular LAM morphologies, respectively. In this study again, we find that the initial transverse LAM ($\bar{L}$) are oriented into parallel, diagonal, and perpendicular alignment as we decrease the frequency v, similar to the case of pure DBCPs under oscillatory shear. However, this time such transverse-to-perpendicular transition takes place at a lower frequency, $v = 1.5 \times 10^{-4}$, than the pure DBCPs case at $v = 2.5 \times 10^{-4}$. On one hand, in these LAM phases of nanocomposites, the orientation behavior of NRs is highly sensitive to the imposed shear flow and immediately oriented to the flow direction, originating from the NRs orientation entropy. On the other hand, the NRs are exclusively distributed within the A phase domains, due to the preferentially attractive interactions between NRs and A monomers of blocks. The latter case is confirmed again by the densities of blocks A, B, and NRs, plotted in Figure 3(a2–d2). Especially in Figures 3(b2,d2), the NRs density curves in yellow present a maximum value at the center of the preferred A block domains, while in B block domains the NRs distribution is close to 0. This can be contributed to that "prevention of configurational entropy loss" still plays a dominant role in controlling the location of selective NRs in polymer matrix. Naturally, A-selective NRs tend to concentrate in A phase domains in energy; however. If the polymer chains try to wrap around the NRs, it will lead to losing significant configurational entropy. Therefore, the chain pushes the A-selective NRs to gather in the center of the A block domains, where most chain ends lie, to decrease the conformational entropy of the polymer chains. These results qualitatively agree with the experimental studies for block copolymer/spherical nanoparticle composites without shear conditions.[44] To illustrate our simulated results without regard to the box size, we also

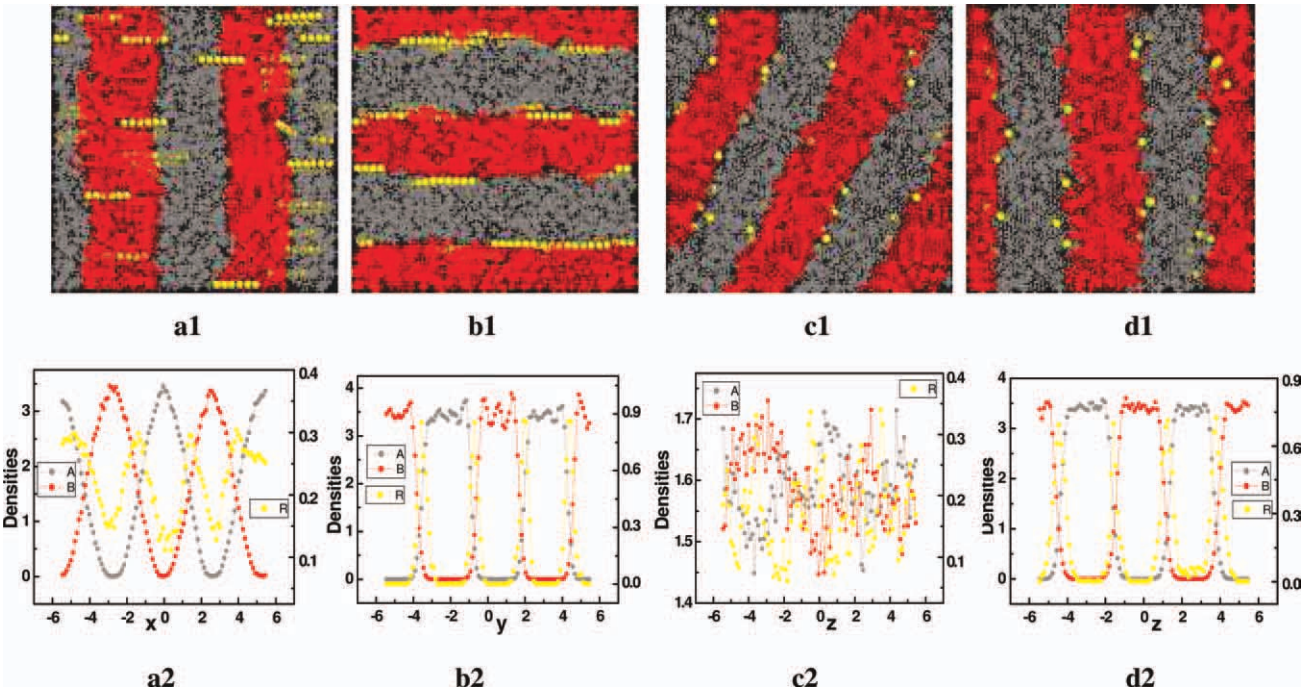

Figure 4. Morphologies and densities of DBCPs/non-selective NRs ($\phi_N = 5\%$) at amplitude $\gamma_0 = 0.1$ and frequencies $v = 1.0 \times 10^{-3}$, 8.0×10^{-4}, 5.0×10^{-4}, 4.0×10^{-4}. The view in (a1–b1) is perpendicular to shear direction, while the view in (c1–d1) is parallel to shear direction. [Color figure can be viewed in the online issue, which is available at wileyonlinelibrary.com.]

simulate the larger DPD system of $V = 13 \times 13 \times 13$, with the same shear amplitude and frequency. The results are shown in Figure 3(a3–d3), well consistent with those for the smaller system of $V = 11 \times 11 \times 11$.

For comparison, we also focus on the mixtures of DBCPs and nonselective NRs, with the same NRs concentration of $\phi_N = 5\%$. In Figure 4(a1–d1), we show simulation snapshots at different frequencies of $v = 1.0 \times 10^{-3}$, 8.0×10^{-4}, 5.0×10^{-4}, and 4.0×10^{-4}, corresponding to transverse LAM, parallel LAM, thinner diagonal LAM, and perpendicular LAM phase, respectively. Again, we see the reorientation transition from initial transverse LAM into parallel, diagonal, and perpendicular alignment as the shear frequency v decreases, except this time transverse-to-perpendicular reorientation takes place at a higher frequency, $v = 4.0 \times 10^{-4}$, than the pure DBCPs case of $v = 2.5 \times 10^{-4}$. Moreover, as shown in Figure 4(a1–d1), the snapshots display the nonselective NRs are mostly centered around the interface between A and B phase domains. From the NRs density curves shown in Figure 4(a2–d2), we can see that the NRs density peaks appear at the A/B interface, obviously in (b2) and (d2). The nonselective NRs show equal enthalpic interactions with either domain (A or B blocks), so the main driving force causing the NRs to position at the A/B interface is the reduction in interfacial tension led by the decrease in the number of A/B contacts.[45] It means that the enthalpy effect overcome the entropy effect dominating the distribution of nonselective NRs in polymer matrix, where the enthalpy depends on the energy interactions between NRs and A (and B) blocks, and the entropy results from the conformation behavior of copolymer chains. Consequently, despite the DBCPs/NRs composites under the shear flow, the competition between entropy and enthalpy involving various components, still dominates the distribution of NRs within polymer fluids.

Noted on the three systems shown in Figures 2–4, as the shear frequency decreases, there are similar reorientation transitions from transverse LAM into parallel, thinner diagonal, and perpendicular alignment, respectively, but this transverse-to-perpendicular reorientation of LAM takes place at different critical frequencies v_c for three systems, that is, $v_c = 2.5 \times 10^{-4}$ for pure DBCPs case, $v_c = 1.5 \times 10^{-4}$ for DBCPs/A-selective NRs case, and $v_c = 4.0 \times 10^{-4}$ for DBCPs/nonselective NRs system, respectively. In short, the presence of selective/nonselective NRs advances or delays the frequency-induced reorientation transition from transverse LAM to perpendicular LAM. For the case of A-selective NRs, the loaded NRs help in bridging different A chains and strengthening the cohesive forces within A domains, further enhancing the segregation $(\chi N)_{eff}$ between blocks A and B. The enhancement of incompatibility between blocks A and B would cause the increasing of order–disorder transition temperature (T_{ODT}), making the corresponding critical frequency $v_c$of transverse-to-perpendicular LAM reorientation much lower. In this study, the effects of transition temperature T_{ODT} on the critical frequency $v_c$is qualitatively consistent with the findings of Satkowski and co-workers,[46] who similarly studied the effects of T_{ODT} on the critical shear rate γ_c in the steady shear case. For the case of nonselective NRs, the loaded NRs prefer to centering at the interface between A and B phase domains, decreasing the interfacial tension σ, and then weakening the segregation $(\chi N)_{eff}$ between A and B blocks. In contrast with the A-selective NRs case, the decrease in A/B incompatibility would cause an increase in the critical frequency v_c.

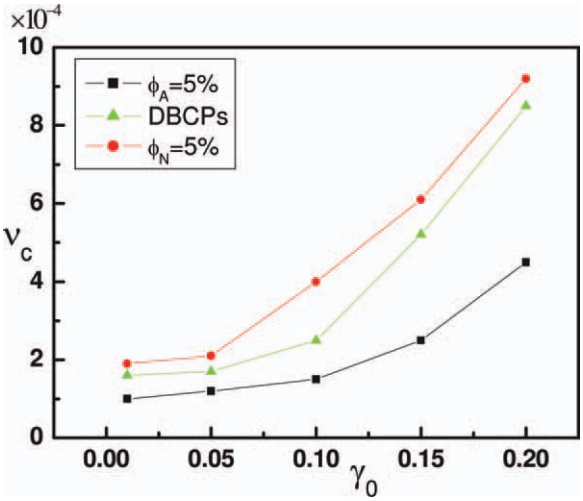

Figure 5. The critical frequency v_c of transverse-to-perpendicular LAM reorientation as a function of amplitude γ_0 for DBCPs melts, DBCPs/A-selective NRs, and DBCPs/nonselective NRs systems. [Color figure can be viewed in the online issue, which is available at wileyonlinelibrary.com.]

In addition, in Figure 5, we present the critical frequency v_c as a function of shear amplitude γ_0 for these three systems (DBCPs melts, DBCPs/A-selective NRs composites, and DBCPs/nonselective NRs composites), which displays the same trend. Take pure DBCPs case (plotted in green) for instance, v_c increases monotonically with shear amplitude γ_0. This result can be interpreted as follows: first, as the frequency continuously decreases, the shear flow eventually induces a LAM reorientation from initially transverse to perpendicular alignment, just corresponding to the critical frequency v_c. Moreover, the more difficulty for such a transition, the lower the corresponding critical frequency v_c. Second, the perpendicular alignment is always preferred at large shear amplitudes γ_0, i.e., the larger shear amplitude γ_0, the easier to complete the shear-induced transverse-to-perpendicular reorientation of LAM. In a word, the increase of shear amplitude γ_0 prompts the transverse-to-perpendicular reorientation of LAM phase, and then leads to an enhancement in the critical frequency v_c of system.

High NRs Concentration

In this part, we turn to consider the composites of DBCPs/A-selective NRs with a high concentration of $\phi_A = 15\%$. Before shearing, the initial LAM phase of nanocomposites is shown in Figure 6(a). Likewise, also select the shear amplitude $\gamma_0 = 0.1$ and decrease shear frequency v. Figure 6(b–d) also display the typical simulated snapshots for DBCPs/NRs composites at different shear frequencies of $v = 5.0 \times 10^{-4}$, 2.0×10^{-4}, and 1.0×10^{-4}, corresponding to parallel LAM, thinner diagonal LAM, and perpendicular LAM phase, respectively. Similar to the low NRs concentration case ($\phi_A = 5\%$), the transitions between the various LAM orientations for these systems also depend on the imposed shear frequency v. At high shear frequency ($v = 5.0 \times 10^{-4}$, b), the LAM tends to align in a parallel configuration, while at low shear frequency ($v = 1.0 \times 10^{-4}$, d), it takes place a transition from transverse to perpendicular alignment, even lower than $v_c = 1.5 \times 10^{-4}$ for $\phi_A = 5\%$ case. It indicates that the more A-selective NRs loaded, the more difficulty such a transverse-to-perpendicular reorientation occurred, suggesting a lower critical frequency v_c. It contributes to the presence of A-selective NRs, which strengthens the cohesive forces within A domains and enhances the segregation $(\chi N)_{eff}$ between blocks A and B, to make the order–order transition more difficult. A close look at Figure 6(d) reveals that the shear-induced NRs orientation is not as uniform as that in parallel and diagonal LAM phases (b, c). It may be interfered by the shear behaviors from polymer chains, which will be discussed in the following more detail.

To compare the different inductions from shear amplitude and frequency on DBCPs/NRs composites, in this study, we also monitor the phase behaviors of nanocomposites at a very low shear frequency of $v = 1.0 \times 10^{-5}$, with varying shear amplitude γ_0 from 0.01 to 0.2. As shown in Figure 7, both the LAM reorientations and morphological transitions are induced by amplitude γ_0, similar to that subjected to the steady shear case.[34] On one hand, the parallel LAM (b) is observed at small shear amplitude of $\gamma_0 = 0.01$ (corresponding to low shear rate), while the perpendicular LAM (h) is observed at large shear amplitude of $\gamma_0 = 0.2$ (corresponding to high shear rate). At some intermediate shear amplitudes, such as

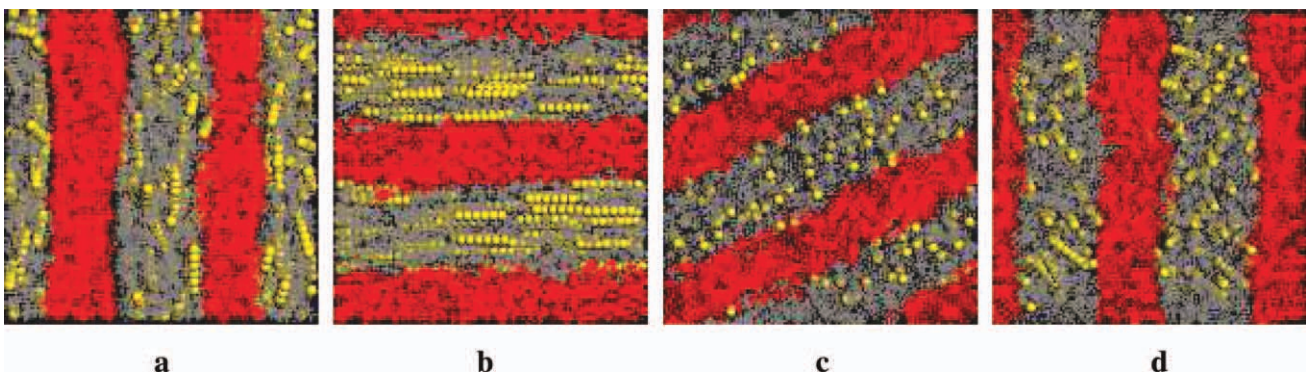

Figure 6. Morphologies of DBCPs/A-selective NRs composites ($\phi_A = 15\%$) at amplitude $\gamma_0 = 0.1$ and frequencies $v = 5.0 \times 10^{-4}$ (b), 2.0×10^{-4} (c), and 1.0×10^{-4} (d). The initial lamellar without shear is shown in (a). The view in (a, b) is perpendicular to shear direction, while the view in (c, d) is parallel to shear direction. [Color figure can be viewed in the online issue, which is available at wileyonlinelibrary.com.]

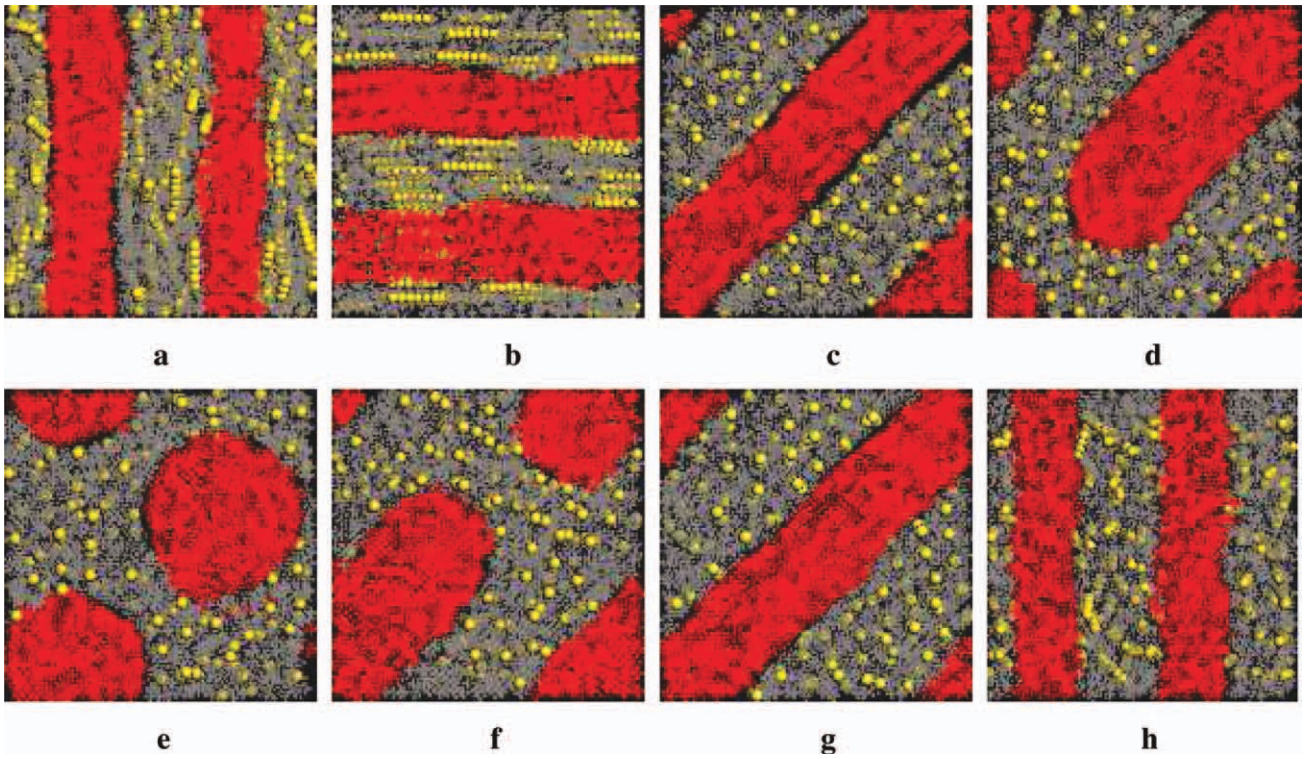

Figure 7. Morphologies of DBCPs/A-selective NRs composites ($\phi_A = 15\%$) at a very low frequency $v = 1.0 \times 10^{-5}$ with varied amplitudes $\gamma_0 = 0, 0.01$, 0.03, 0.05, 0.07, 0.1, 0.15, and 0.2 in (a–h). The view in (a, b) is perpendicular to shear direction, while the view in (c, h) is parallel to shear direction. [Color figure can be viewed in the online issue, which is available at wileyonlinelibrary.com.]

$\gamma_0 = 0.03$ and 0.15(c and g), there are diagonal LAM phases. Interestingly, besides the reorientations in various LAM (parallel, diagonal, and perpendicular alignment), the shear-induced phase structure undergoes a reversible transition: from lamellar to ribbon to cylindrical structure with increasing from $\gamma_0 = 0.01$ to 0.07 shown in Figure 7(b–e), and then conversely from cylindrical to ribbon to lamellar phase with further increasing from $\gamma_0 = 0.07$ to 0.2 shown in Figure 7(e–h). The ribbon structure can be took as a transient phase between lamellar and cylindrical phase.[28] Obviously, the final phase structures of DBCPs/selective NRs composites depend on the interplays between shear-induced behaviors involving polymer and NRs, such as sheared alignment and sheared thinning of chain molecules, and sheared dispersion of NRs, respectively. To further elucidate the differences in phase behaviors of composites induced by shear amplitude and frequency, in the following we focus on the properties of NRs and polymers on the molecule level, respectively.

The positional distribution of particles within polymer matrix can be measured by the pair correlation function $g(r)$, which is related to the probability of finding the position of a particle at a given distance from another particle. For short distances, this is related to how the particles are packed together; for large distances, it is related to the density—a more dense system has more particles. Therefore, the pair correlation function $g(r)$ is normalized by the density and defined as[47]

$$g(r) = \frac{V}{N^2}\left\langle \sum_i \sum_j \delta(r - r_{ij}) \right\rangle \tag{12}$$

where N is the number of particles, $\delta(r)$ is the Dirac delta function, and $\langle * \rangle$ means the ensemble average. Here, once imposed by the shear, NRs would be well oriented to flow direction (i.e., x-axis), so we evaluate the 2D pair correlation function $g(r_{yz})$ by counting the head-particle position of the rod projected in yz-plane, instead of 3D pair correlation function $g(r)$. The corresponding $\langle \sum \sum \delta(r - r_{ij}) \rangle$ is the total number of pairs, whose distance in the yz-plane ranges from r_{yz} to $r_{yz} + \Delta r_{yz}$. In this study, r_{yz} is ranged from 0 to $\sqrt{2}L$ and divided into 30 parts. i.e., $\Delta r_{yz} = \sqrt{2}L/30$, where L represents the size of simulated box. Obviously, the value of $g(r_{yz})$ in ranged from L to $\sqrt{2}L$ is far lower than that in ranged from 0 to L, because of the radial statistics used in cubic box. Corresponding to the shear frequency-induced parallel LAM regions shown in Figure 6(b), the NRs pair correlation function $g(r_{yz})$ are plotted in Figure 8(a), with decreasing frequency from $v = 7.0 \times 10^{-4}$ to 5.0×10^{-4} to 3.0×10^{-4}. The $g(r_{yz})$ curves are basically coincident, which suggests the shear frequency v shows no influence on the NRs dispersion in polymer matrix. This is quite different from the steady shear case, where it has also been shown through both simulations[48] and experiments[49] that dispersion of particles is very sensitive to the shear rate. To further support this

Applied Polymer SCIENCE

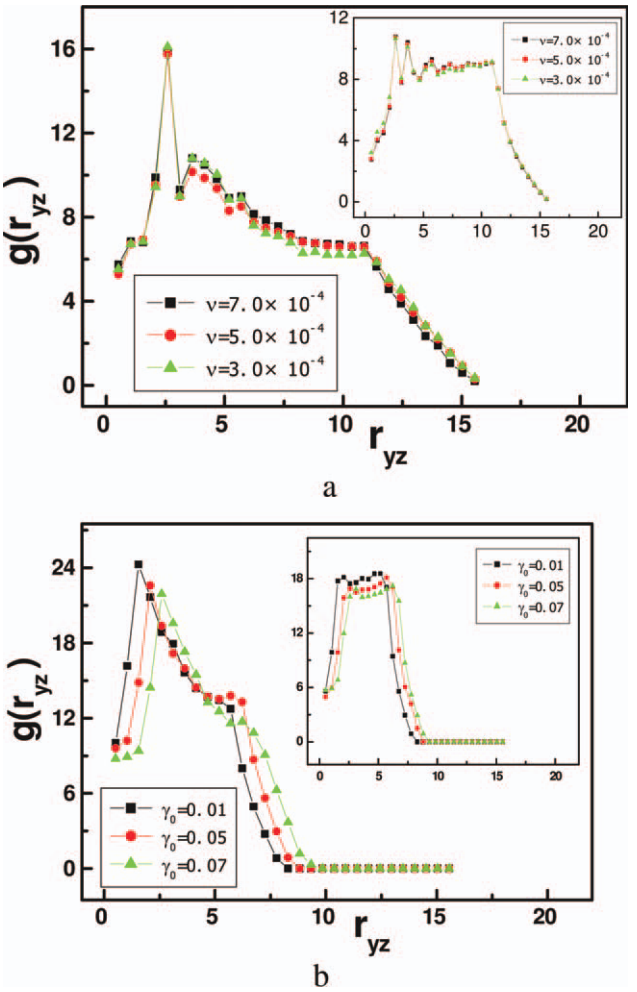

Figure 8. NRs pair correlation function $g(r_{yz})$. (a) $\gamma_0 = 0.1$ and varied v, corresponding to Figure 6; (b) $v = 1.0 \times 10^{-5}$ with varied $\gamma_0 = 0.01$, 0.05, and 0.07, corresponding to parallel lamellar, ribbon, and cylindrical phase shown in Figure 7, respectively. The inset corresponds to the case of homopolymers (A_{10})/A-selective NRs mixtures. [Color figure can be viewed in the online issue, which is available at wileyonlinelibrary.com.]

argument that the irrelevance of NRs dispersions to shear frequency, we also plot $g(r_{yz})$ for homopolymers/NRs composites under the same oscillatory shear, by replacing A_5B_5 DBCPs with A_{10} homopolymers. As shown in the inset of Figure 8(a), with decreasing v from 7.0×10^{-4} to 5.0×10^{-4} to 3.0×10^{-4}, three curves for $g(r_{yz})$ are also well in coincidence, further confirming the NRs spatial dispersion is irrespective of shear frequency v.

In contrast, at a low frequency of $v = 1.0 \times 10^{-5}$ with increasing the shear amplitude from $\gamma_0 = 0.01$ to 0.2, both reorientations and morphological transitions of composites are clearly shown in Figure 7. In this study, the corresponding $g(r_{yz})$ functions at different shear amplitudes of $\gamma_0 = 0.01$, 0.05, and 0.07 are also plotted in Figure 8(b), corresponding to the parallel LAM, ribbon, and cylindrical structures in Figure 7(b, c, and e), respectively. With increasing the amplitude from $\gamma_0 = 0.01$ to 0.05 to 0.07, the significant right shift of peaks in $g(r_{yz})$ curves is observed, which suggests the NRs become dispersed as amplitude increases. Meanwhile, the corresponding average distance inter-NRs d_r is calculated as 2.08, 2.50, and 2.67, respectively, illustrating the NRs in cylindrical phase ($\gamma_0 = 0.07$ and $d_r = 2.67$) are more dispersed than that in LAM phase ($\gamma_0 = 0.01$ and $d_r = 2.08$). In addition, $g(r_{yz})$ for homopolymers/NRs composites with the same shear amplitudes of $\gamma_0 = 0.01$, 0.05, and 0.07, are displayed in the inset of Figure 8(b). Therefore, it can be inferred that with increasing the amplitude, the NRs dispersion is improved firstly, and consequently the dispersion is basically stabilized at a large amplitude or even larger, in well consistent with that from the studies on the spherical nanoparticles incorporated in shear-flow polymer fluids.[48] In summary, the shear-induced NRs dispersion is sensitive to amplitude but irrespective of frequency.

Combining Figure 6 with Figure 8(a), no frequency-induced NRs dispersion is observed, so there is no phase transition except the LAM reorientation, where the latter is mainly caused by the effects of shear flow on the polymer chains, such as alignment, stretched, and thinning behaviors, as mentioned in pure DBCPs case. Meanwhile, based on Figures 7 and 8(b), we will further analysis the phase behaviors of DBCPs/NRs composites with varying shear amplitude. As shown in Figure 7, at small amplitudes ($\gamma_0 = 0.01$ to 0.07), amplitude-induced dispersion of NRs in preferred A domain equivalently increases the A effective composition of the chains (f_A), which is responsible for the phase transitions from lamellar to cylindrical phases (b–e). At large amplitudes ($\gamma_0 = 0.07 - 0.02$), the amplitude-induced polymer thinning dominates and in turn tightens NRs dispersion, i.e., equivalently decrease the A effective composition (f_A), which is responsible for the reverse phase transitions from cylindrical back to lamellar structures (e–h). Therefore, the amplitude-induced phase behaviors, including the LAM reorientations and morphological transition, cooperatively depend on the interplay between sheared polymers and sheared NRs behaviors.

The orientation behavior of NRs can be measured quantitatively as follow:

$$\langle P(\cos\theta)\rangle = \left\langle (3\cos^2\theta - 1)/2 \right\rangle \tag{13}$$

where θ is the angle between NRs orientation and the imposed shear direction (i.e., x-axis). The average NRs orientation $\langle P(\cos\theta)\rangle$ will take values of −0.5, 0, and 1 for NRs that are perpendicular, randomly oriented and parallel to x-axis. Figure 9(a) shows the average NRs orientation $\langle P(\cos(\theta))\rangle$ as a function of shear frequency for different amplitudes. At small shear amplitude, such as $\gamma_0 = 0.01$ and 0.05, the value of $\langle P(\cos(\theta))\rangle$ is always close to 1.0, showing NRs are well oriented to flow direction and irrespective of frequency. When γ_0 is increased up to 0.1 or even to 0.15, the frequency has a significant affect on NRs orientation. With the frequency decreasing, the value of $\langle P(\cos(\theta))\rangle$ decreases and drops obviously at some frequency. For example, $\gamma_0 = 0.1$, $\langle P(\cos(\theta))\rangle$ drops obviously at the frequency of 1.0×10^{-4}, just corresponding to the orientation flip to perpendicular alignment. In other words, a relatively evident drop of $\langle P(\cos(\theta))\rangle$ takes place at a transition of transverse-to-

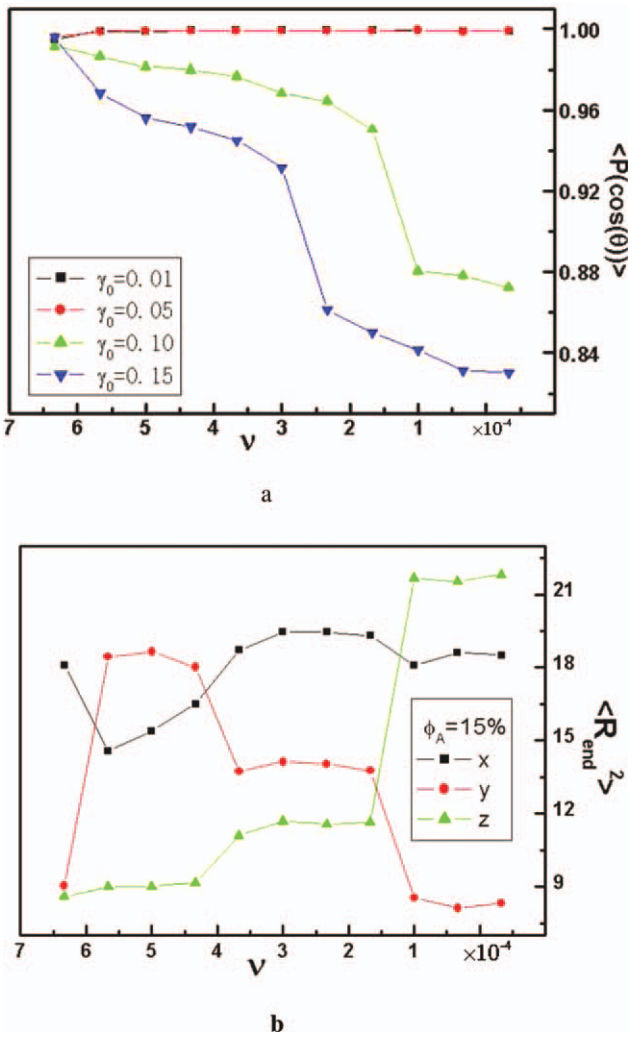

Figure 9. (a) Average NRs orientation $\langle P(\cos(\theta))\rangle$. (b) Mean-squared end-to-end distance of copolymer chains in the *x*-, *y*-, and *z*-direction for $\gamma_0 = 0.1$. [Color figure can be viewed in the online issue, which is available at wileyonlinelibrary.com.]

perpendicular LAM alignment. As expected, the NRs orientation is highly sensitive to the external fields. Once imposed by shear flow, all NRs would be oriented uniformly to the flow direction, due to the inherent NRs orientation entropy. However, combining Figure 6(d) with Figure 9(a), we can see that the shear-induced NRs orientation is slightly perturbed, more obvious at large shear amplitude and low shear frequency. It can be inferred that there is a competition between the NRs orientation and chain alignment with respect to the flow direction (i.e., *x*-axis). Also take $\gamma_0 = 0.1$ for example, Figure 9(b) shows the mean-squared end-to-end distance of copolymer chains $\langle R^2_{end}\rangle$ in *x*-, *y*-, and *z*-directions as a function of shear frequency *v*. At a high frequency, such as $v = 6.5 \times 10^{-4}$, $\langle R_x^2\rangle > \langle R_y^2\rangle \approx \langle R_z^2\rangle$ shows that the initial transverse LAM structure is remained. The stretched directions of chain molecule is along to x-axis, which is consistent well with shear-induced NRs orientation, therefore mutually resulting in a high value of $\langle P(\cos\theta)\rangle$. As frequency decreases, the initial transverse LAM phase is oriented to parallel, diagonal, and finally perpendicular alignment, respectively. Correspondingly, the stretched direction of copolymer chain is converted into y- axis and z-axis, while the NRs orientation always prefers to align to flow direction. The stretched chains will energetically perturb the uniform NRs orientations, leading to a decrease in $\langle P(\cos(\theta))\rangle$. It is slightly obvious in perpendicular LAM regions, such as $v = 1.0 \times 10^{-4}$, in which $\langle R_z^2\rangle > \langle R_x^2\rangle > \langle R_y^2\rangle$. However, this disturbs from shear-stretched polymer chains do not plays leading role in $\langle P(\cos(\theta))\rangle$ of NRs, which is still mainly determined by the imposed shear flow, simultaneously also dependent on the confinement of LAM phase region and the intrinsic isotropic-nematic (IN) transition behaviors. After all, the NRs orientation is highly sensitive to the imposed flow, originating from the inherent NRs orientation entropy. In a word, these observations show the spatial orientation of NRs not only directly depends on the imposed shear and the confinement from LAM phase region, but also is slightly affected by the shear-stretched alignment of copolymer molecules.

Finally, in Figure 10, we display the simulated snapshots of DBCPs/nonselective NRs systems with the NRs concentration of $\phi_N = 15\%$. The LAM reorientations are also similar to the case of $\phi_N = 5\%$, while the transverse-to-perpendicular transition takes places at $v = 6.0 \times 10^{-4}$, even higher than $v_c = 4.0 \times 10^{-4}$ for $\phi_N = 5\%$ case. This result can be interpreted that with the increase of NRs distribution at the A/B interface domains, causing the further reduction in segregation $(\chi N)_{eff}$ between blocks A and B, makes the order–order transition easier and therefore enhances the critical frequency v_c. Obviously, the sheared NRs are oriented to flow direction and enthalpically centered round the A/B interface; meanwhile, the alignment of chain molecule will change with shear frequency. Therefore, for the DBCPs melts mixed with nonselective NRs, the oscillatory shear also does not induce the phase transitions except the LAM reorientations of nanocomposites. In addition, we also investigate the effects of shear flow on the rheological properties of nanocomposites. Figure 11 shows the viscosity η as a function of the shear frequency *v* for pure DBCPs melts, DBCPs/A-selective NRs, and DBCPs/nonselective NRs systems, respectively. First, overall the viscosity η decreases with the shear frequency decreasing, which is consistent with the experimental results obtained by Raghavan et al.[50] Take the pure DBCPs melts(plotted in green) for example, the shear viscosity gradually decreases following a transverse-to-parallel and transverse-to-diagonal transition, and sharply drops at the critical frequency of $v_c = 2.5 \times 10^{-4}$, indicating an orientation flip into perpendicular LAM phase. In our simulations, $\eta_{\text{perpendicular}}$ is smaller than η_{parallel}, which is in agreement with the experimental results that the shear viscosity relates to the orientation of the LAM phase.[51] Second, the addition of A-selective NRs increases the system viscosity η monotonically with the NRs concentration, while nonselective NRs with varied concentrations show no dramatic effects on the rheological behavior of systems. As mentioned above, the A-selective NRs are mostly pushed toward the center of the preferred domain, where most chain ends lie, and help in bridging different chains, which play as the "network nodes," causing the percolating polymer network reinforcement.

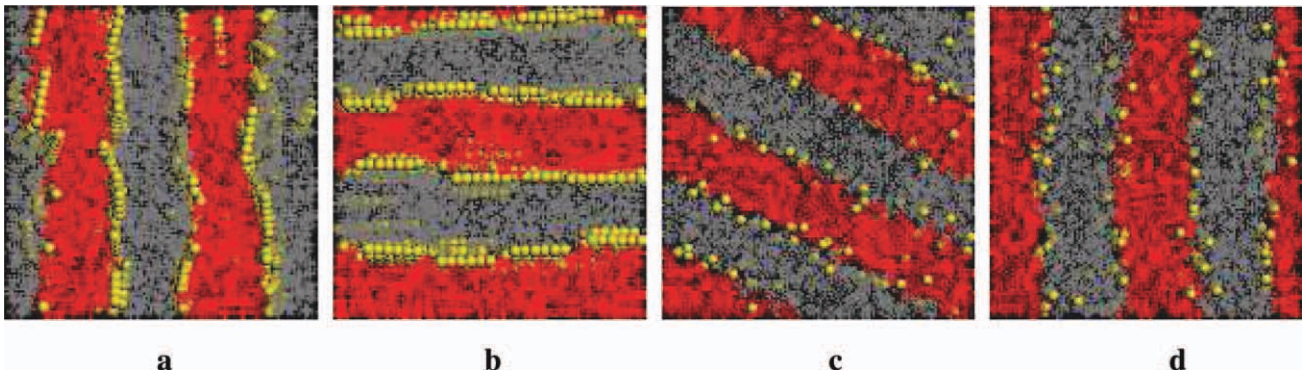

Figure 10. Morphologies of DBCPs/nonselective NRs composites ($\phi_N = 15\%$) at amplitude $\gamma_0 = 0.1$ and frequency $v = 9.0 \times 10^{-4}$, 7.5×10^{-4}, and 6.0×10^{-4} in (b, c). The initial lamellar without shear is shown in (a). The view in (a, b) is perpendicular to shear direction, while the view in (c, d) is parallel to shear direction. [Color figure can be viewed in the online issue, which is available at wileyonlinelibrary.com.]

Consequently, the presence of selective NRs enhances the fluids viscosity by bridging polymer chains at the chain ends, while it is ineffective to the case of nonselective NRs centered in A/B interface.

CONCLUSIONS

We have conducted DPD simulations on how oscillatory shear flow affects the phase behaviors of lamellar DBCPs melts and lamellar DBCPs/NRs composites. The rich LAM reorientations and morphological transitions of systems are induced by shear amplitude and shear frequency. To preserve LAM morphology in the nanocomposites, we control NRs concentration below 15% divided into three cases: pure DBCPs, low NRs concentration, and high NRs concentration. For pure DBCPs melts, we roughly construct a LAM orientation diagram as a function of shear amplitude and frequency. In general, the LAM orientation depends on both amplitude and frequency. For example, at a constant shear amplitude, as varying shear frequency, the initial transverse LAM is oriented successively to parallel, diagonal, and perpendicular LAM phases, respectively. Then we focus on DBCPs/NRs composites subjected to oscillatory shear. Both selective and nonselective NRs are considered, which are classified by their affinities with the diblocks of copolymer chains.

For low NRs concentration (such as $\phi_{A(N)} = 5\%$), we find the shear frequency-induced LAM reorientation of composites, well consistent with that of DBCPs melts. The only difference among DBCPs melts, DBCPs/selective NRs and DBCPs/nonselective NRs composites is the critical frequency of transverse-to-perpendicular LAM reorientation, which is determined by the distribution of NRs within polymer fluids, such as NRs located in preferred domains or unbiased interface domains. Despite the nanocomposites under the nonequilibrium conditions (i.e., imposed by shear), the interplay between entropy and enthalpy involving each component (blocks A, B, and NRs), still dominates the location of NRs within polymer matrix. In addition, this critical frequency also increases with shear amplitude increasing. For high NRs concentration (such as $\phi_{A(N)} = 15\%$), we separately compare the different inductions on DBCPs/NRs composites caused by shear frequency and amplitude. The final phase structure of composites depends on the competition between respective shear-induced behaviors involving polymer chains and NRs. The shear frequency just induces the LAM reorientation without morphological transition, which is contributed to that the NRs dispersion is irrespective of frequency but sensitive to amplitude. In contrast, the shear amplitude-induced phase behaviors of composites are rich, including the sheared thinning of chains and sheared dispersion of NRs, which are cooperatively responsible for the reversible morphological transitions between lamellar and cylindrical phases.

In addition, the orientation behavior of NRs not only directly depends on the imposed shear flow but also is interfered by the shear-stretched alignment of chain molecules. Meanwhile, the rheological properties of systems depend on the shear frequency, the concentration, and surface property of NRs. In summary, the oscillatory shear can be used as a useful method to control the self-assembly of nanocomposites, including the phase behaviors of NRs within polymer fluids.

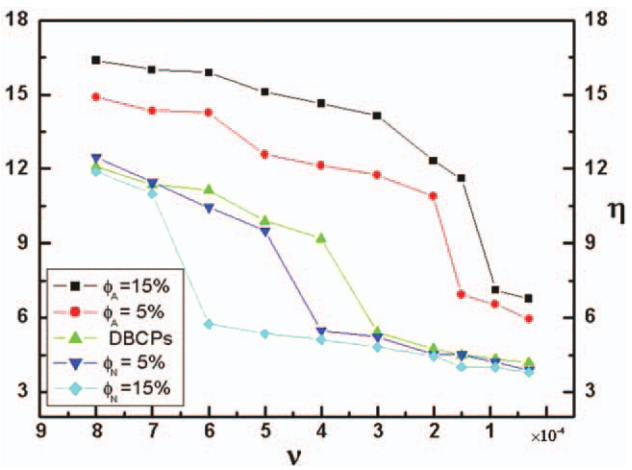

Figure 11. The shear viscosity η as a function of the frequency v for DBCPs melts, DBCPs/A-selective NRs, and DBCPs/nonselective NRs systems. [Color figure can be viewed in the online issue, which is available at wileyonlinelibrary.com.]

ACKNOWLEDGMENTS

This research was financially supported by the National Natural Science Foundation of China (Nos. 20974081, 20934004, 21074096, and 21104060).

REFERENCES

1. Hajduk, D. A.; Harper, P. E.; Gruner, S. M.; Honeker, C. C.; Thomas, E. L.; Fetters, L. J. *Macromolecules,* **1995,** *28*, 2570.
2. Likhtman, A. E.; Semenov, A. N. *Macromolecules,* **1997,** *30*, 7273.
3. Feng, J.; Ruckenstein, E. J. *Chem. Phys.,* **2004,** *121*, 1609.
4. Pinna, M.; Zvelindovsky, A. V.; Todd, S.; Goldbeck-Wood, G. J. *Chem. Phys.,* **2006,** *125*, 154905.
5. Guo, H.; Kremer, K. J. *Chem. Phys.,* **2007,** *127*, 054902.
6. Guo, H. J. *Chem. Phys.,* **2006,** *124*, 054902.
7. Lísal, M.; Brennan, J. K. *Langmuir,* **2007,** *23*, 4809.
8. Fraser, B.; Denniston, C.; Müser, M. H. *J. Chem. Phys.,* **2006,** *124*, 104902.
9. You, L.; Chen, L.; Qian, H.; Lu, Z. *Macromolecules,* **2007,** *40*, 5222.
10. Luo, K.; Yang, Y. *Macromolecules,* **2002,** *35*, 3722.
11. Hamley, I. W. *J. Phys.: Condens. Mater.,* **2001,** *13*, R643.
12. Koppi, K. A.; Tirrell, M.; Bates, F. S.; Almdal, K.; Colby R. H. *J. Phys. II,* **1992,** *2*, 1941.
13. Hadziioannou, G.; Mathis, A.; Skoulios, A. *Colloid Polym. Sci.,* **1979,** *257*, 136.
14. Zhang, Y.; Wiesner, U.; Spiess, H. W. *Macromolecules,* **1995,** *28*, 778.
15. Maring, D.; Wiesner, U. *Macromolecules,* **1997,** *30*, 660.
16. Wiesner, U. *Macromol. Chem. Phys.,* **1997,** *198*, 3319.
17. Fritz, G.; Wagner, N. J.; Kaler, E. W. *Langmuir,* **2003,** *19*, 8709.
18. Chen, P. *Phys. Rev. E,* **2005,** *71*, 061503.
19. Morozov, A. N.; Fraaije, J. G. E. M. *Phys. Rev. E,* **2002,** *65*, 031803.
20. You, L.; He, Y.; Zhao, Y.; Lu, Z. J. *Chem. Phys.,* **2008,** *129*, 204901.
21. Ji, S.; Ding, J. J. *Chem. Phys.,* **2005,** *122*, 164901.
22. Peng, G.; Qiu, F.; Ginzburg, V. V.; Jasnow, D.; Balazs, A. C. *Science,* **2000,** *288*, 1802.
23. Lopes, W. A.; Jaeger, H. M. *Nature (Lond), 2001*, 414, 735.
24. Huynh, W. U.; Dittmer, J. J.; Alivisatos, A. P. *Science,* **2002,** *295*, 2425.
25. Greene, L. E.; Law, M.; Yuhas, B. D.; Yang, P. J. *Phys. Chem. C,* **2007,** *111*, 18451.
26. Zhang, Q. L.; Gupta, S.; Emrick, T.; Russell, T. P. *J. Am. Chem. Soc.,* **2006,** *128*, 3898.
27. Tang, Q.; Ma, Y. J. *Phys. Chem. B.,* **2009,** *113*, 10117.
28. He, L.; Zhang, L.; Liang, H. *Polymer,* **2010,** *51*, 3303.
29. Kalra, V.; Mendez, S.; Escobedo, F.; Joo, Y. L. *J. Chem. Phys.,* **2008,** *128*, 164909.
30. Mendoza, C.; Pietsch, T.; Gindy, N.; Fahmi, A. *Adv. Mater.,* **2008,** *20*, 1179.
31. Mendoza, C.; Gindy, N.; Gutmann, J. S.; Frömsdorf, A.; Förster, S.; Fahmi, A. *Langmuir,* **2009,** *25*, 9571.
32. Pozzo, D. C.; Walker, L. M. *Eur. Phys. J. E.,* **2008,** *26*, 183.
33. Pozzo, D. C.; Walker, L. M. *Macromolecules,* **2007,** *40*, 5801.
34. He, L.; Pan, Z.; Zhang, L.; Liang, H. *Soft Mater.* **2011,** *7*, 1147.
35. Pan, Z.; He, L.; Zhang, L.; Liang, H. *Polymer,* **2011,** *52*, 2711.
36. Hoogerbrugge, P. J.; Koelman, J. M. V. A. *Europhys. Lett.,* **1992,** *19*, 155.
37. Groot, R. D.; Madden, T. J. *J. Chem. Phys.,* **1998,** *108*, 8713.
38. AlSunaidi, B. A.; den Otter, W. K.; Clarke, J. H. *R. Philos. Trans. R. Soc. Lond.* **2004,** *362*, 1773.
39. Groot, R. D.; Warren, P. B. *J. Chem. Phys.,* **1997,** *107*, 4423.
40. Allen, M. P.; Tildesley, D. J. Computer Simulations of Liquids; Clarendon Press: Oxford, **1987.**
41. Raos, G.; Moreno, M.; Elli, S. *Macromolecules,* **2006,** *39*, 6744.
42. Jiang, W. H.; Huang, J. H.; Wang, Y. M.; Laradji, M. J. *Chem. Phys.,* **2007,** *126*, 044901.
43. Komatsugawa, H.; Nosé, S. J. *Chem. Phys.,* **2000,** *112*, 11058.
44. Bockstaller, M. R.; Lapetnikov, Y.; Margel, S.; Thomas, E. L. *J. Am. Chem. Soc.* **2003,** *125*, 5276.
45. Schultz, A. J.; Hall, C. K.; Genzer, J. *Macromolecules,* **2005,** *38*, 3007.
46. Chen, Z. R.; Kornfield, J. A.; Smith, S. D.; Grothaus, J. T.; Satkowski, M. M. *Science,* **1997,** *277*, 1248.
47. Satoh, A.; Chantrell, R. W.; Kamiyama, S. I.; Coverdale, G. N. *J. Colloid Interface Sci.,* **1996,** *181*, 422.
48. Kalra, V.; Escobedo, F.; Jooa, Y. L. *J. Chem. Phys.,* **2010,** *132*, 024901.
49. Kairn, T.; Daivis, P. J. *J. Chem. Phys.,* **2005,** *123*, 194905.
50. Raghavan, S. R.; Khan, S. A. *J. Colloid Interface Sci.,* **1997,** *185*, 57.
51. Zipfel, J.; Lindner, P.; Tsianou, M.; Alexandridis, P.; Richtering, W. *Langmuir,* **1999,** *15*, 2599.